PIF7 controls leaf cell proliferation through an AN3 substitution-39 repression mechanism

PIF7 controls leaf cell proliferation through an AN3 substitution repression mechanism

Ejaz Hussain[a], Andrés Romanowski[a], and Karen J. Halliday[a,1]

[a]Institute of Molecular Plant Sciences, School of Biological Sciences, University of Edinburgh, Edinburgh 3H9 3BF, United Kingdom

Edited by Peter Quail, Department of Plant and Microbial Biology, University of California, Berkeley, CA; received August 25, 2021; accepted December 7, 2021

Plants are agile, plastic organisms able to adapt to everchanging circumstances. Responding to far-red (FR) wavelengths from nearby vegetation, shade-intolerant species elicit the adaptive shade-avoidance syndrome (SAS), characterized by elongated petioles, leaf hyponasty, and smaller leaves. We utilized end-of-day FR (EODFR) treatments to interrogate molecular processes that underlie the SAS leaf response. Genetic analysis established that PHYTOCHROME-INTERACTING FACTOR 7 (PIF7) is required for EODFR-mediated constraint of leaf blade cell division, while EODFR messenger RNA sequencing data identified *ANGUSTIFOLIA3* (*AN3*) as a potential PIF7 target. We show that PIF7 can suppress *AN3* transcription by directly interacting with and sequestering AN3. We also establish that PIF7 and AN3 impose antagonistic control of gene expression via common *cis*-acting promoter motifs in several cell-cycle regulator genes. EODFR triggers the molecular substitution of AN3 to PIF7 at G-box/PBE-box promoter regions and a switch from promotion to repression of gene expression.

AN3 | PIF7 | EODFR | leaf development | cell proliferation

Growth plasticity is a fundamental property of plants, enabling adjustment to changes in the environment. The shade-avoidance syndrome (SAS) is a well-known adaptive response to the presence of nearby vegetation that is characterized by gross changes in plant architecture and biomass (1–3). A common feature of SAS is the reduction in leaf blade growth, which can be dramatic in heavy vegetation shade. Our recent research and that of others has shown that phytochrome, an important modulator of the SAS leaf response, operates by controlling cell proliferation and expansion phases of development (4–6). The molecular mechanisms through which phytochrome controls leaf growth are, however, unresolved.

In *Arabidopsis*, phytochromes comprise a small gene family (PHYA to E) of photochromic biliproteins that are tuned to detect far-red (FR) light-rich conditions which occur in vegetation-dense habitats (7, 8). The photo-isomeric properties of phytochrome dictate that red (R) light wavelengths drive the photoconversion from the inactive Pr to the active Pfr isomeric form. Exposure to FR wavelengths reverses this process, switching phytochrome to its inactive Pr state. Several studies have shown that FR inactivation of phyB-E set in motion a series of molecular signaling events that activate SAS (7). Although SAS is principally regulated by phyB, phyC has a contributory role, while phyD and phyE operate redundantly with phyB in this response (7, 9). In contrast, phyA signaling, which is enhanced by extended periods of FR, acts to limit the extent of SAS, which can be detrimental if left unchecked (10).

PhyB is known to operate by negatively regulating the PHYTOCHROME-INTERACTING FACTOR (PIF) class of bHLH transcription factors. Studies indicate phyB can inhibit PIF1 and PIF3 action through sequestration and can also initiate phosphorylation-mediated proteasomal degradation of PIF1, PIF3, PIF4, and PIF5 (11–13). Consequently, the deactivation of phyB by FR light leads to PIF de-repression and activation of transcriptional events. Of these PIFs, PIF4 and PIF5 have prominent roles in SAS alongside another family member, PIF7, which has somewhat distinct regulatory characteristics. For instance, the phosphorylated form of PIF7 is not degraded; rather, it is retained in the cytosol through interaction with 14-3-3 proteins (14). FR-rich shade light induces PIF7 dephosphorylation and translocation to the nucleus.

An important SAS feature is the physiological response to FR is gated by the circadian clock with a peak in FR responsiveness at dusk (15, 16). This property means that end-of-day FR (EODFR) treatments are effective in eliciting SAS (6, 17). Furthermore, the delivery of short EODFR treatments avoids activating the SAS suppressor phyA, assisting the delivery of a robust SAS response (7, 18). Recent reports have shown that PIF7 has a prominent role in mediating SAS responses induced by EODFR and that its action is clock gated (15, 16, 19). FR shade light leads to the rapid activation of PIF7 through dephosphorylation and nuclear accumulation (14, 19, 20). These distinct molecular properties mean PIF7-mediated SAS signaling can be swiftly deployed following phyB deactivation at dusk, particularly on short days when PIF7 is reported to be most effective (19). After an EODFR treatment, PIF7 is primarily active post-dusk, as rising levels of the night-phased clock component ELF3 gradually suppress PIF7 action through direct interaction and the prevention of PIF7 DNA binding (21).

Earlier studies demonstrated that simulated canopy shade can constrain the phase of leaf cell proliferation in a process involving HD-Zip II transcription factors *ATHB2* and *ATHB4* (5, 22). Our recent messenger RNA sequencing (mRNA-seq) analysis identified key leaf development genes as EODFR regulated, revealing a signaling route through which phytochrome

Significance

Phytochrome photoreceptors can markedly alter leaf blade growth in response to far-red (FR) rich neighbor shade, yet we have a limited understanding of how this is accomplished. This study identifies ANGUSTIFOLIA3 (AN3) as a central component in phytochrome promotion of leaf cell proliferation and PHYTOCHROME-INTERACTING FACTOR 7 (PIF7) as a potent repressor. AN3 and PIF7 impose opposing regulation on a shared suite of genes through common *cis*-acting promoter elements. In response to FR light, activated PIF7 blocks AN3 action by evicting and substituting for AN3 at target promoters. This molecular switch module provides a mechanism through which changes in external light quality can dynamically manipulate gene expression, cell division, and leaf size.

Author contributions: E.H., A.R., and K.J.H. designed research; E.H. and A.R. performed research; E.H. contributed new reagents/analytic tools; E.H., A.R., and K.J.H. analyzed data; E.H. and K.J.H. wrote the paper; and A.R. reviewed and edited the manuscript.

The authors declare no competing interest.

This article is a PNAS Direct Submission.

[1]To whom correspondence may be addressed. Email: karen.halliday@ed.ac.uk.

This article contains supporting information online at http://www.pnas.org/lookup/suppl/doi:10.1073/pnas.2115682119/-/DCSupplemental.

Published January 27, 2022.

controls leaf growth (6). Among these genes, *ANGUSTIFOLIA 3*/*GRF-INTERACTING FACTOR 1* (*AN3*/*GIF1*), *GROWTH-REGULATING FACTORs GRF2*, *GRF4*, and *GFR6*, and *BRAHMA* (*BRM*) are known to regulate leaf blade cell proliferation, while the small, narrow leaf phenotype of the *an3-4* mutant is reminiscent of the *phyB* leaf blade phenotype (23–26). AN3 is proposed to operate centrally in a complex with DNA-binding GRFs and with SWITCH/SUCROSE NONFERMENTING (SWI/SNF) chromatin remodeling proteins such as BRM and BAF60 to regulate transcription (26). Interestingly the AN3–GRF–SWI/SNF complex is highly conserved in eudicots and monocots and therefore represents a widespread leaf development mechanism (27–29).

This study delineates a molecular mechanism that links phytochrome signaling to leaf development. We establish PIF7 is a potent inhibitor of leaf cell proliferation following SAS-inducing EODFR treatments. Genetic analysis indicates this is accomplished through the repression of AN3. We show PIF7 suppresses *AN3* expression through a sequestration mechanism that prevents AN3 self-activation. Our data also point to PIF7 and AN3 signaling convergence at common promoter *cis*-elements in cell-cycle genes. EODFR induces PIF7 substitution for AN3 at target promoters and a concomitant shift from promotion to the repression of gene expression.

Results

EODFR Inhibits Cell Division during Distinct Phases of Leaf Development. Previously, we used phytochrome-deactivating EODFR treatments to mimic and test the impact of vegetative shading at different phases of rosette leaf 3 (L3) development (6). We established that daily EODFR was effective in limiting L3 expansion by suppressing epidermal cell division or expansion, contingent on whether EODFR coincided with the proliferation or expansion phase of development. Extending these findings, we found that EODFR treatment delivered daily (light:dark [LD] 12-h:12-h photoperiod at 22 °C) from day 6, or *phyB-9*, are equally effective in reducing the cell number but not the size of both epidermal and palisade cells (*SI Appendix*, Fig. S1). We observed similar EODFR effects on leaf blade expansion for all rosette leaves (*SI Appendix*, Fig. S2) but focus on L3 as a model to allow a direct comparison to our published data and other studies (6, 30–32).

To pinpoint more precisely the time window during which phytochrome controls blade cell division, we exposed plants grown in a LD 12-h:12-h photoperiod at 22 °C to 5 d of EODFR in the following intervals: days 6 to 10, 10 to 14, or 14 to 18; negative controls did not receive EODFR, and positive controls received EODFR for days 6 to 18 or 6 to 34 (Fig. 1). As expected, EODFR delivered for the longest period, 6 to 34 d, was the most effective in reducing the blade area and limiting cell division followed by the 6 to 18 and 10 to 14 intervals (Fig. 1 *B*–*H*). EODFR treatments provided in the 6- to 10- or 14- to 18-d windows elicited very modest reductions in cell number when compared to the 10- to 14-d window, which was as effective as the longer 6- to 18-d period. Concurring with our previous study, the EODFR treatments, all initiated relatively early on in leaf development, do not lead to changes in the cell size of both epidermal and palisade cells (Fig. 1 *D* and *G*) (6). The data identify two main windows on which phyB controls cell division: days 10 through 14, which coincides with the main proliferative phase, and days 18 through 34, which coincides with the meristemoid cell division phase (33).

mRNA-Seq Identifies EODFR-Regulated Genes Implicated in Cell-Cycle Control. As the molecular connections between phyB and cell-cycle control are largely unknown, we sought to identify candidate cell-cycle regulator genes during the primary proliferative growth phase from our L3 mRNA-seq data (6). This longitudinal study captured EODFR-induced changes in transcription through leaf development. From this dataset, we identified 317 genes classified as transcription factors or cotranscriptional regulators (Dataset S1), with EODFR-altered expression early on in L3 development. In this gene set, 14 genes (*AN3*, *GRF2*, *GRF4*, *GRF6*, *DP-E2FA like1*, *AINTEGUMENTA*, *DP-E2F like3*, *FAMA*, *SCARECROW*, *AT4G02110*, *HOMEOBOX GENE 8*, *AUXIN RESPONSE FACTOR 10*, *ASYMMETRIC LEAVES 1*, and *MYB DOMAIN PROTEIN 3R-4*) are known to have roles associated with the cell cycle (24, 34, 35). In nearly all cases, expression levels were higher on day 13, which falls in the 10- to 14-d window that coincides with cell proliferation in our experimental regime (*SI Appendix*, Fig. S3 *A*–*C*) (6) (https://aromanowski.shinyapps.io/leafdev-app/).

Recent articles have identified AN3 as a key regulator of leaf growth, controlling cell-cycle duration and the timing of differentiation (25, 26, 36, 37). AN3 occupies a central position in a transcriptional complex where it forms a bridge between SWI/SNF chromatin remodeling complexes and GRFs to direct BRM (or SPLAYED [SYD]) ATPase activity and gene transcription (26). Our finding indicates the AN3 transcriptional module could potentially operate downstream of phytochrome to control leaf cell division and growth.

EODFR Regulation of Cell Division is Abolished in the *an3-4* Mutant. To establish if AN3 is implicated in phytochrome control of the cell cycle, we first analyzed the EODFR leaf response in the *an3-4* mutant. In line with earlier reports (25, 36), in our conditions, *an3-4* L3 blades were smaller than wild type (WT) with fewer cells (Fig. 2 *A* and *B* and *SI Appendix*, Fig. S4*B*). We found *an3-4* was still EODFR responsive, but the treatment was less effective in *an3-4*, reducing blade area by 40% compared to 51% in the WT (Fig. 2*A*). In contrast, while EODFR markedly reduced WT epidermal and palisade cell number, *an3-4* was completely insensitive to the treatment (Fig. 2*B* and *SI Appendix*, Fig. S4*B*). We also established that, similar to an earlier study (38), in our control conditions, *an3-4* epidermal and palisade cells were slightly larger than WT (*SI Appendix*, Fig. S4 *A* and *C*). However, EODFR application completely suppressed the *an3-4* cell size defect (*SI Appendix*, Fig. S4). This finding most likely accounts for the retention of the small blade area EODFR response in the *an3-4* mutant. Since AN3 complexes with GRFs, which are reported to have redundant roles in regulating leaf size, we analyzed the EODFR responsiveness of multi-allele *grf* mutants (24). We found that the triple *grf1-3;grf3-1;grf5-2* and quadruple *grf1-3;grf3-1;grf4-1;grf5-2* mutants are indistinguishable from *an3-4* for leaf blade and cellular responses (Fig. 2 *A* and *B* and *SI Appendix*, Fig. S4). In summary, our data show *an3-4* and multi-allele *grf* mutants have a constitutively low cell number and are insensitive to EODFR, which implies the AN3 complex may operate downstream of phytochrome to promote leaf blade cell division. In addition, our data indicate that phytochrome inactivation by EODFR prevents cell expansion caused by AN3 or GRF deficiency.

AN3 is Required for phyB-Controlled Expression of Leaf Cell-Cycle Regulators. Several of the leaf developmental genes identified as EODFR repressed in our mRNA-seq dataset are known AN3 targets (6, 26, 28, 34). For instance, previous reports have shown AN3 can associate with the *GRF6* promoter using chromatin immunoprecipitation (ChIP) qPCR and with *GRF2*, *GRF4*, *OLIGOCELLULA 2* (*OLI2*), *SALT TOLERANCE ZINC FINGER* (STZ), and *BRM* promoters using tandem chromatin affinity purification sequencing (TChAP-seq) or ChIP-seq (26, 28). Furthermore, the overexpression of *AN3* resulted in increased expression of *CYCB1;1*, identifying this cell-cycle gene as AN3 regulated (26, 34). We reasoned that if the phytochrome-controlled cellular response is mediated through AN3, then EODFR control of

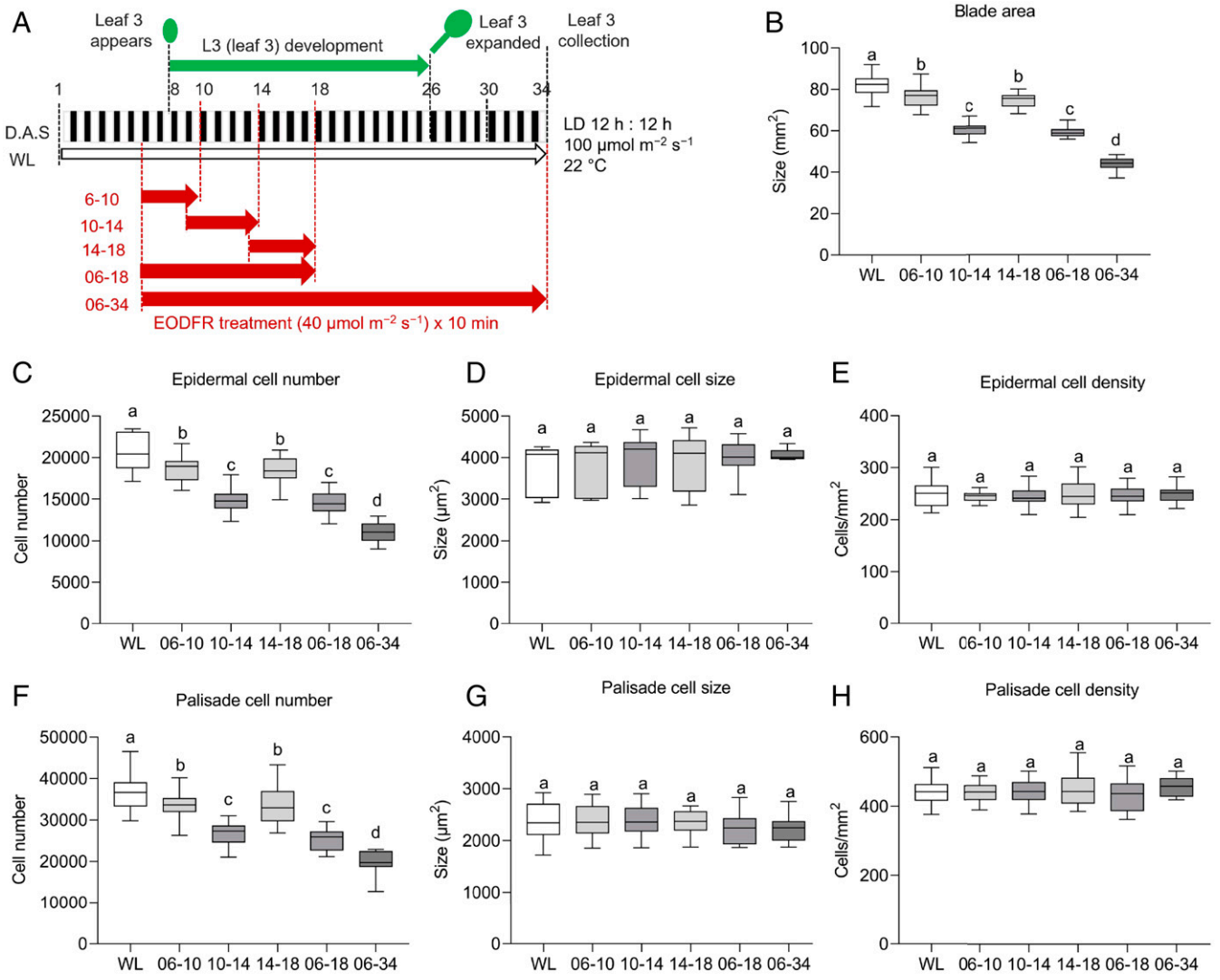

Fig. 1. EODFR inhibits cell division during distinct phases of leaf development. (*A*) Schematic representation of L3 development and the light treatment regime. The green arrow indicates the period of L3 development, days are shown above a series of white and black rectangles representing 12:12-h day–night cycles. L3 emergence occurs at day 8, full blade expansion at day 28, and samples were taken on day 34. The WL arrow indicates control 12L:12D conditions, red arrows show the different treatment periods during which the plants received daily EODFR for 10 min after dusk. (*B*) L3 blade area (*B*), epidermal (*C*–*E*), and palisade (*F*–*H*) cell number, size, and cell density in plants subject to EODFR for days 6 to 10, 10 to 14, 14 to 18, 6 to 18, or 6 to 34. Box plot central lines represent the mean, and whiskers show minimum and maximum values. Different letters denote statistically significant differences between treatments from one-way ANOVA followed by Tukey's post hoc test, $P < 0.0001$ (*B*, *C*, and *F*); $P < 0.6200$ (*D*), $P < 0.8435$ (*G*); $P < 0.6023$ (*E*), $P < 0.9604$ (*H*), ($n > 20$ blades, ~27 cells per blade). Experiments were replicated at least three times with similar results.

these AN3 targets would be curtailed in the *an3-4* mutant. Indeed, compared to WT, our qRT-PCR assay showed that this gene set has reduced expression in *an3-4* and was completely unresponsive to EODFR (Fig. 2*C*). This was also the case for the AN3 targets *GRF1*, *GRF3*, and *GRF5* and key cell-cycle genes *CDC45* and *CDC6* identified as EODFR repressed in our mRNA-seq data (*SI Appendix*, Fig. S3*D*) (6) but not previously known to be AN3 regulated (*SI Appendix*, Fig. S4*F*) (26). These data identify *CDC45* and *CDC6* as AN3 regulated and support the hypothesis that AN3 action is promoted by phytochrome. Our results suggest AN3 promotes the expression of genes that modulate the leaf cell cycle in control conditions but not in EODFR, which deactivates phyB and other SAS-controlling phytochromes.

AN3 Operates Downstream of PIF7 to Control Leaf Cell Division. PIF7 is known to have an important function in EODFR-induced seedling and adult plant responses, while the contribution from other PIFs is smaller (16, 19, 39). Consistent with this notion, we show *pifq*, which lacks PIF1, PIF3, PIF4, and PIF5 and has a smaller leaf blade area with fewer epidermal cells in control conditions but still responds to EODFR, although the response is reduced (*SI Appendix*, Fig. S5). In contrast, *pif7-1* has a WT leaf blade size and is completely unresponsive to EODFR, which is consistent with previous findings (40) (Fig. 3*A*). Likewise, the *pif7-1* mutant has a similar epidermal cell number and cell size to WT white light control and lacks the EODFR reduction in cell number (Fig. 3 *B*–*D*). These data reflect the known functional properties of PIF7, which is activated by EODFR, and additionally illustrate that PIF7 is necessary for the EODFR suppression of phytochrome-mediated leaf cell proliferation (19).

As we have shown that AN3 promotion of cell proliferation is prevented by EODFR, our data implicate PIF7 as a negative regulator of AN3. To begin to test this hypothesis, we generated the *an3-4;phyB-9*, *an3-4;pif7-1*, and *an3-4;phyB-9;pif7-1* multi-allele

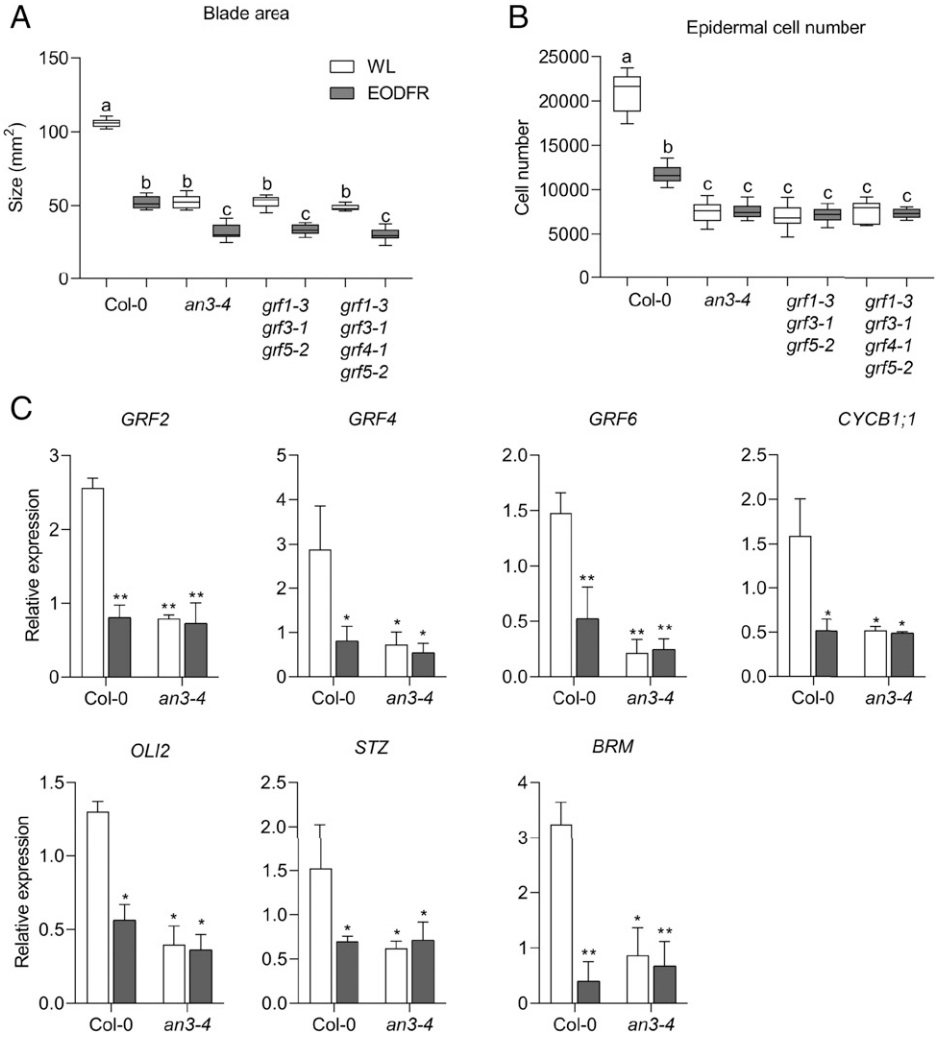

Fig. 2. The *an3-4* mutant is completely insensitive to EODFR regulation of leaf cell division. (*A*) Leaf blade area and (*B*) epidermal cell number in Col-0 (WT), *an3-4*, *grf1-3;grf3-1;grf5-2*, and *grf1-3;grf3-1;grf4-1;grf5-2* in WL (12L:12D) control and EODFR (6 to 34) conditions at 22 °C. Box plot central lines represent the mean, and whiskers show minimum and maximum values. Different letters denote statistically significant differences between genotypes and treatments from one-way ANOVA followed by Tukey's post hoc test, $P < 0.05$ ($n = 14$ blades). (*C*) Expression of *GRF2*, *GRF4*, *GRF6*, *CYCB1;1*, *OLI2*, *STZ*, and *BRM* in Col-0 (WT) and *an3-4*, measured by RT-qPCR in WL (12L:12D) control and EODFR conditions (from day 6) at 22 °C. Samples were taken from 13-d-old seedlings at zeitgeber (ZT) 14. The transcript levels were calculated relative to those of *PP2A*. Error bars represent the SD of three biological replicates: Student's *t* test significance $*P < 0.05$, $**P < 0.01$, and $***P < 0.001$.

mutants. Fig. 3 *A* and *B* show that, as expected, *phyB-9* L3 blades are smaller and narrower than those of WT with reduced epidermal cell number in control conditions, while *pif7-1* lacks a WT response to EODFR. Comparison of cell number in *an3-4;phyB-9*, *an3-4;pif7-1*, *an3-4;phyB-9;pif7-1* and the single-mutant parental lines, revealed *an3-4* epistasis over *phyB-9* which was most evident in control conditions, and *an3-4* epistasis over *pif7-1*, particularly under EODFR. Thus, AN3 appears to be required for phyB-PIF7 module control of leaf cell division.

With regards to L3 epidermal cell size, *phyB-9* and *pif7-1* are indistinguishable from the WT, and as shown earlier, *an3-4* cells are larger in control but not in EODFR conditions (Fig. 3 *C* and *D*). In contrast to cell number, for cell size, *phyB-9* is epistatic to *an3-4* in control conditions, and *pif7-1* is epistatic to *an3-4* in EODFR, indicating that *an3-4* cell expansion is dependent on whether phyB is active. Furthermore, *an3-4;phyB-9;pif7-1* is indistinguishable from *an3-4:pif7-1* (Fig. 3*A*), which is consistent with PIF7 operating downstream of phyB. Collectively, our data indicate that AN3 is required for the phyB promotion of cell division in control conditions. EODFR induced PIF7 activation and restricts cell division, possibly by repressing AN3 levels and/or activity, and secondarily, PIF7 appears to limit the compensatory cell expansion that arises from AN3 deactivation.

PIF7 Suppresses *AN3* Expression through Direct Binding to the *AN3* Promoter. Our mRNA-seq data showed *AN3* transcript abundance is lowered by EODFR, and our genetic data identified PIF7 as a potential *AN3* regulator (6). To test this, we quantified *AN3* transcript levels in *pif7-1* by qRT-PCR assay. Fig. 4*A* shows *AN3* transcript levels are unaltered by EODFR in *pif7-1*, which implicates PIF7 as a repressor of *AN3* transcription. A recent study reported that, as for other PIFs, PIF7 preferentially binds to G-boxes (CACGTG) and PBE-boxes (CA[TG/CA]TG) in the promoters of target genes (41). Interestingly, in *Arabidopsis*, a G-box motif has been identified as an important transcriptional *cis*-regulatory element in the *AN3* promoter; thus, we surmised PIF7 may directly regulate *AN3* transcription (42). To test this, we performed ChIP-qPCR assays using 13-d-old leaf tissues of WT and PIF7-Flash (*35S::PIF7-Flash*; 9xMyc-6xHis-3xFlag) plants (20). This assay showed PIF7-FLASH enrichment at the G-box–containing region of the *AN3* promoter (P1), which was

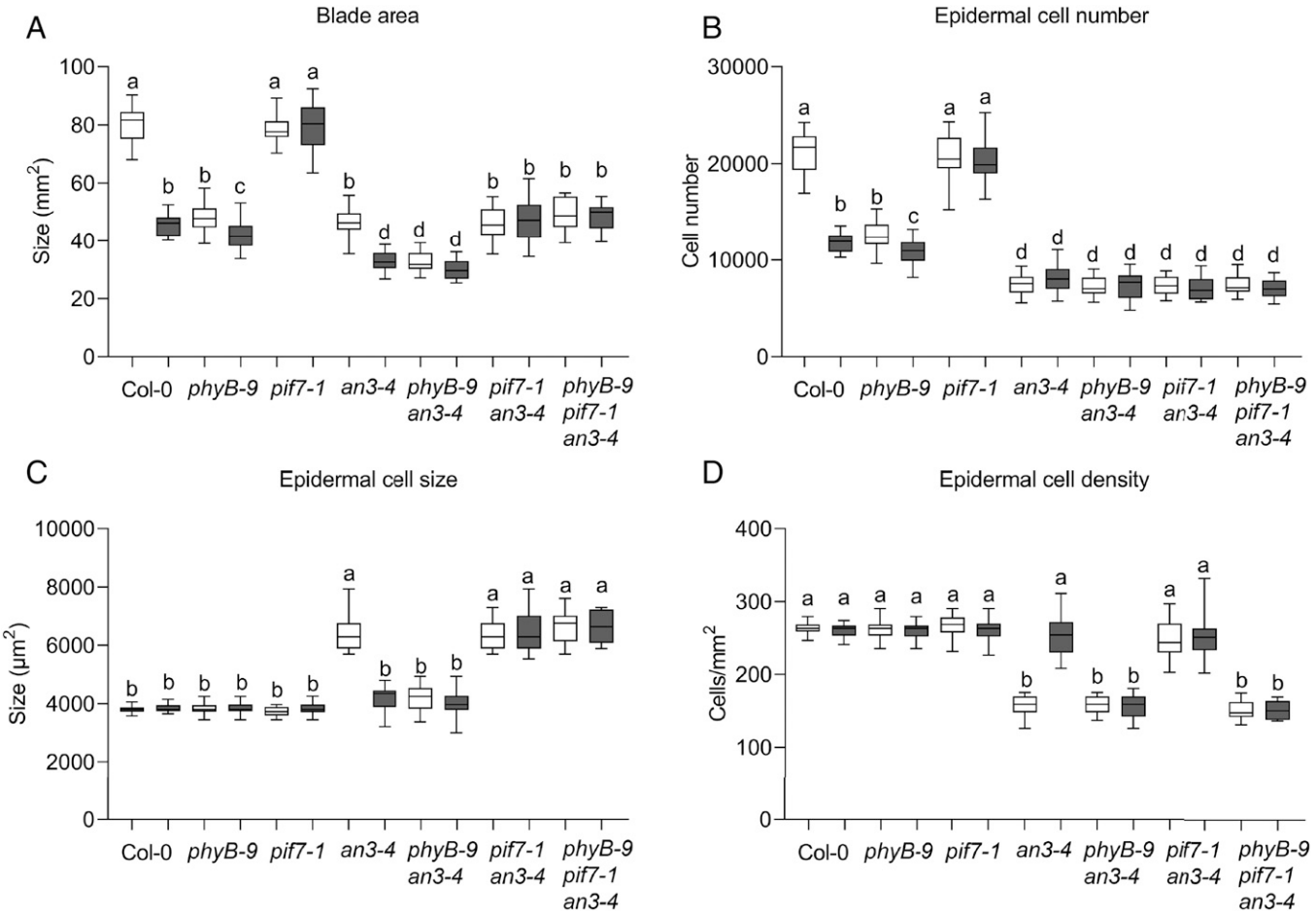

Fig. 3. The *an3-4* allele is epistatic to *pif7-1* for EODFR control of cell number. (*A*) L3 blade area, (*B–D*) Epidermal cell number, size, and density of Col-0 (WT), *phyB-9*, *pif7-1*, *an3-4*, *phyB-9;an3-4*, *pif7-1;an3-4*, *phyB-9;pif7-1;an3-4*, in WL (12L:12D) control and EODFR (6 to 34) conditions at 22 °C. Box plot central lines represent the mean, and whiskers show minimum and maximum values. Different letters denote statistically significant differences in leaf blade area, cell number, cell size, and cell density between genotypes and treatments (one-way ANOVA followed by Tukey's post hoc test, $P < 0.05$).

further enhanced after EODFR (Fig. 4*C*). Increased PIF7 binding following EODFR is consistent with the retention of an EODFR leaf response in the 35S::PIF7-FLASH line (Fig. 4*E*). We also recorded PIF7-FLASH enrichment at the G-box–containing promoter region of the known PIF7 target, *IAA19* but not in either of the negative controls, a fragment of the AN3 coding DNA sequence (CDS) (P4) and a no-antibody control (Fig. 4*D*) (43). These observations, together with the *AN3* expression data, (Fig. 4*A*) indicate that PIF7 directly represses *AN3* expression through association with the G-box region (P1) of the *AN3* promoter.

EODFR Prevents AN3 Binding to Its Own Promoter. We reasoned that if PIF7 was operating through *AN3* to regulate leaf blade cell proliferation, then PIF7 would also be required for the EODFR suppression of AN3 target genes. This is indeed what we observed, as for each of the AN3 regulated genes (*GRF1*, *GRF2*, *GRF3*, *GRF4*, *GRF5*, *GRF6*, *CYCB1;1*, *OLI2*, *STZ*, *BRM*, *CDC45*, and *CDC6*), *pif7-1* completely abolished the EODFR repression response (*SI Appendix*, Fig. S6). Next, we tested if PIF7 functions solely by regulating *AN3* expression by establishing if the EODFR response was attenuated in a 35S::AN3-GS^{yellow} line (28). Consistent with published data, we found that the 35S::AN3 line had elevated *AN3* expression and a moderately increased leaf blade area in control conditions (Fig. 4*E* and *SI Appendix*, Fig. S7 *A* and *C*) (28). However, this line exhibited a WT response to EODFR, suggesting PIF7 may not regulate AN3 solely by modulating its transcription; rather, it might also regulate AN3 activity.

Published studies indicate AN3 can bind to its own promoter to promote expression through self-regulatory motifs (the GAGA motif present in the region encoding the 5′ untranslated region [UTR] and a CATGTT box) in the *AN3* promoter (26, 44) (Fig. 4*B*). As PIF7 has not been shown to bind to these motifs, we used ChIP-qPCR to test if PIF7 activation by EODFR disrupts AN3 association with self-regulatory motifs. As expected, we observed statistically significant enrichment of 35S::AN3 (Student's *t* test; *P* values < 0.001) at the GAGA (P2) and CATGTT-containing regions (P3) but not the *AN3* coding sequence control (P4) (Fig. 4 *F* and *G*). Notably, we did not observe 35S::AN3 association with P2 or P3 following EODFR. We next tested if PIF7 could bind to these regions using PIF7-Flash–expressing plants and found that, while we detected PIF7 enrichment at the promoter of a known target, *IAA19* (Student's *t* test; *P* value < 0.001), PIF7 did not associate with regions containing the GAGA or CATGTT motifs in control or EODFR conditions (Fig. 4 *F* and *G*). Furthermore, EODFR-induced AN3 eviction from the GAGA region (P2) is dependent on the presence of PIF7, as AN3 enrichment is observed in EODFR in the *pif7-1* mutant (Fig. 4*H*). Thus, our data indicate that, in response to EODFR, PIF7 prevents AN3 association with self-regulatory elements in its own promoter and 5′ UTR.

To test if PIF7 interacted directly with AN3, we conducted in vitro pull-downs using extracts from 35S::PIF7-Flash and 35S::AN3-GS^{yellow} lines and in vivo coimmunoprecipitation (co-IP) assays with a line coexpressing 35S::PIF7-Flash and

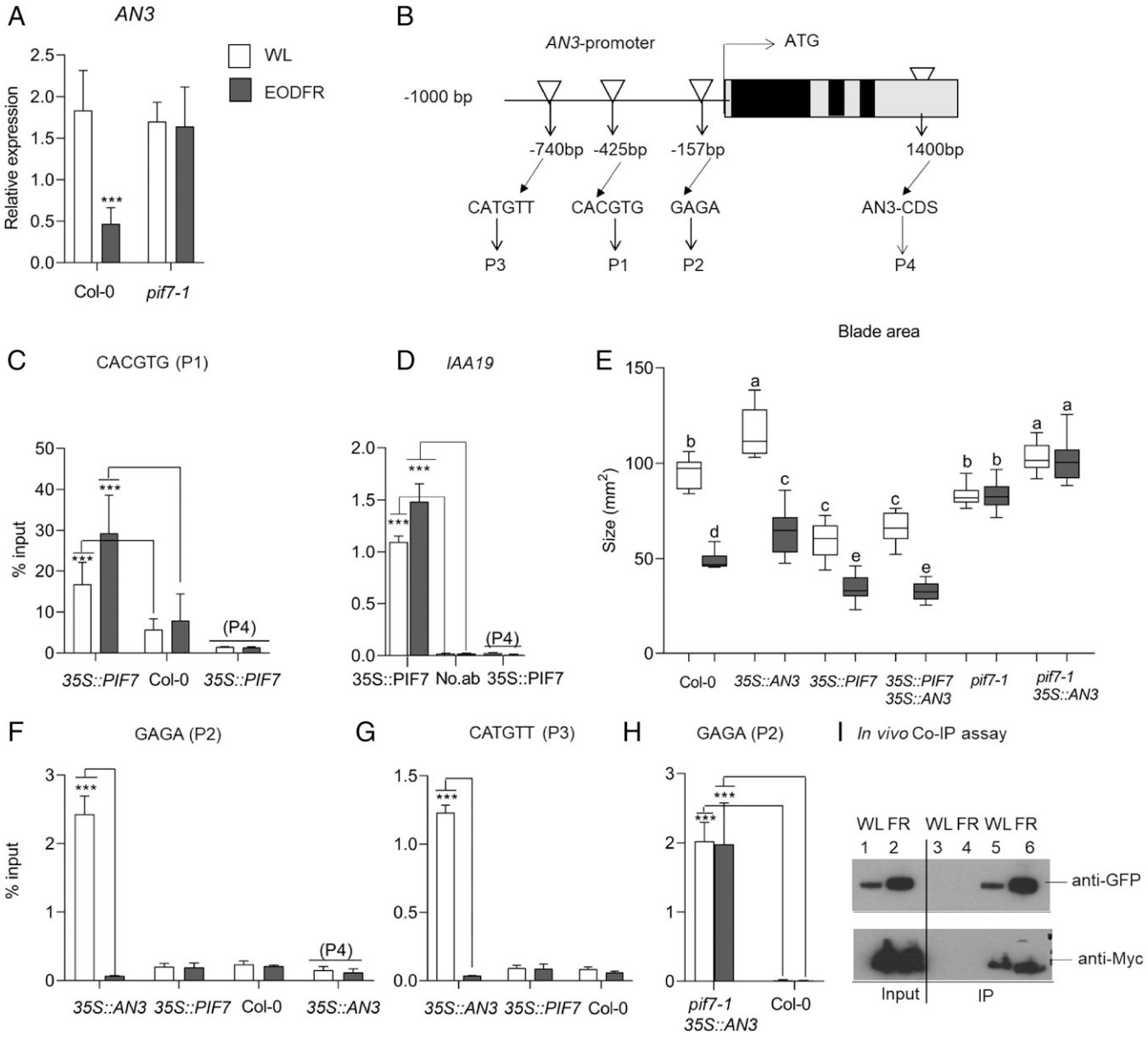

Fig. 4. PIF7 directly suppress *AN3* expression to restrict leaf growth. (*A*) *AN3* mRNA levels in Col-0 (WT) and *pif7-1* in WL (12L:12D) and EODFR determined by RT-qPCR. (*B*) Schematic showing the locations of promoter/UTR elements P1 (G-box: CACGTG), P2 (GAGA), P3 (CATGTT), and the P4 CDS region. (*C* and *D*) ChIP-qPCR assays showing differences of PIF7-FLASH enrichment at *AN3* P1 and the G-box region of the *IAA19* promoter in control and EODFR. Enrichment in the *35S::PIF7-FLASH (35S::PIF7)* line is compared to Col-0 (WT), *AN3* P4 (CDS), and no antibody (no ab) controls. (*E*) L3 blade area in Col-0 (WT), *35S::AN3*^{yellow}, *35S::PIF7-FLASH*, *35S::PIF7-FLASH;35S::AN3*^{yellow}, *pif7-1*, *pif7-1; 35S::AN3*^{yellow}. Box plot central lines represent the mean, and whiskers show minimum and maximum values. Different letters denote statistically significant differences between treatments from one-way ANOVA followed by Tukey's post hoc test, $P < 0.0001$; $n > 12$ blades. (*F–H*) ChIP-qPCR assays showing differing levels of AN3^{yellow} enrichment at P2, P3 in control and EODFR, and PIF7-dependent enrichment at P2. Enrichment in the *35S::AN3*^{yellow} *(35S::AN3)* line is compared to Col-0 (WT) and *AN3* P4 (CDS) controls. (*I*) In vivo co-IP of AN3 and PIF7 in WL and EODFR (FR). Samples were taken at ZT14 from a *35S::PIF7-FLASH;35S::AN3* ^{yellow} line and an anti-Myc antibody was used to precipitate PIF7-FLASH. The immunoblot shows input (lanes 1 and 2) and precipitated fractions (lanes 5 and 6) using anti-GFP and anti-Myc antibodies. Lanes 3 and 4 are precipitated fractions from the *35S::AN3* ^{yellow} line using anti-Myc antibody used as negative control. For RT-qPCR and ChIP data, samples were taken at ZT14 from 13-d-old seedlings grown at 22 °C; mean values are shown, error bars represent the SD of three biological replicates (*$P < 0.05$, **$P < 0.01$, and ***$P < 0.001$, Student's *t* test).

35S::AN3-GS^{yellow} (Fig. 4*E* and *SI Appendix*, Fig. S7*C*). For both assays, we found that AN3^{yellow} coimmunoprecipitated with PIF7-Flash in the white light (WL) control and after EODFR (Fig. 4*I* and *SI Appendix*, Fig. S7*B*). The interaction in control conditions is consistent with the increased levels and activity of PIF7, evidenced by the small L3 blade of the *35S::PIF7-Flash* line, which is comparable to EODFR treated WT plants (Fig. 4*E* and *SI Appendix*, Fig. S7*C*). Interestingly, we also observed slightly higher levels of AN3 protein in EODFR, which implies that either AN3 protein synthesis or degradation is altered by EODFR (Fig. 4*I*). Taken together, our results suggest EODFR conditions promote PIF7 action and sequestration of the AN3 complex from target leaf cell-cycle gene promoters. The suppressive action of PIF7 over AN3 is also evident in the *pif7-1*; 35S::AN3 line, where leaf blades are unresponsive to EODFR, and the double overexpression line, where 35S::PIF7 completely represses the 35S::AN3 larger blade phenotype in both control and EODFR conditions (Fig. 4*E* and *SI Appendix*, Fig. S7*C*).

EODFR Induces a Switch from AN3 to PIF7 at Common Target Promoters. Close inspection of previously published (AN3-HBH TChAP-seq) data revealed high-confidence AN3 protein binding peaks in gene promoter regions containing GAGA, PBE-box (CA[TG/CA]TG), and G-box motifs, while ChIP-qPCR assay confirmed AN3 binding on PBE-boxes of *GRF5* and *GRF6* promoters (27). Furthermore, our *cis*-acting regulatory DNA element analysis showed that *AN3* itself, and all the AN3 regulated genes in this study, possessed G-box (CACGTG) and/or PBE-box promoter motifs (*SI Appendix*, Fig. S8). This finding provided the possibility that AN3 and PIF7 signaling may converge at these *cis*-elements in a common set of genes. Indeed, using ChIP-qPCR, we observed a PIF7-FLASH and AN3^{yellow} enrichment at G-box and or PBE-box promoter regions in *AN3*, *GRF2*, *GRF4*, *GRF6*, *CYCB1;1*, *OLI2*, *STZ*, *GRF1*, *GRF3*, *GRF5*, *CDC45*, and *CDC6* in control but not in EODFR conditions (Fig. 5*A* and *SI Appendix*, Fig. S9*A*). For most of these genes, EODFR enhanced PIF7-FLASH enrichment but markedly reduced AN3^{yellow} association with G-box/PBE-box regions (Fig. 5 *A* and *B* and *SI Appendix*, Fig. S9 *A* and *B*). However, in the *pif7-1;*35S::AN3 line, we observed AN3 enrichment at G-box/PBE-box regions under control and EODFR conditions (Fig. 5*C* and *SI Appendix*, Fig. S9*C*). Collectively, our analysis indicates that AN3 and PIF7 antagonistically regulate a common set of genes that control leaf cell proliferation. EODFR leads to the activation of PIF7, the removal of AN3 from *cis*-regulatory elements, and PIF7 substitution for AN3 at G-box– or PBE-box–containing regions of target promoters.

Discussion

SAS is an important survival strategy that enables plants to adapt to and thrive in FR-rich, and often light depleted, vegetation environments. A prominent feature of SAS is the marked reduction in leaf size, which is brought about by restricting cell proliferation and/or expansion (4–6, 22). PhyB is known to play a pivotal role in orchestrating these changes in leaf development, yet current knowledge of how this is elicited is scant. This study brings a molecular level, mechanistic understanding of how phytochrome signaling is coupled to leaf blade cell division. We demonstrate that when phyB is active, cell proliferation is promoted by AN3, but, following phyB deactivation by EODFR, PIF7 blocks AN3 action by preventing AN3 complexing at target promoters (Fig. 5*D*).

In this work, we applied phy-deactivating EODFR at different intervals through L3 development and identified two main periods during leaf development (10 to 14d and 18 to 34d postgermination) during which phyB controls cell division (Fig. 1 *B–H*). These two phases correspond to the initial period of cell division that precedes cell expansion and differentiation and the later meristemoid phase of cell proliferation (45, 46). We then used mRNA-seq data to identify EODFR-controlled regulators of early cell proliferation, among which we found *AN3*, *GRF2*, *GRF4*, and *GRF6* (*SI Appendix*, Figs. S3 *A–C* and S10). Previous work had shown that AN3 interacts directly with SWI/SNF complexes and GRFs to regulate cell proliferation (26, 29, 47). We were therefore interested to establish if phyB control of leaf expansion is mediated through the AN3 complex. Indeed, our genetic analysis supported this notion, as, like *phyB-9*, *an3-4*, and high order *grf*, mutants had small L3 blades with a reduced cell number and insensitivity to EODFR (Figs. 2 *A* and *B* and 3 *A* and *B*). As GRFs are known to have functional redundancy, our data points to a potentially central role for AN3 in phyB-mediated control of L3 cell division.

It is well documented that the FR deactivation of phyB leads to the activation and/or accumulation of PIF transcription factors and that PIF7 is the principal EODFR responder (16, 19). Our genetic data confirm this and illustrate that PIF7 operates by limiting cell proliferation. Furthermore, *pif7-1;an3-4* double-mutant analysis showed complete *an3-4* epistasis over *pif7-1* under EODFR, indicating that PIF7 likely operates by repressing AN3 action. In agreement with previously published reports (25, 36), we also observed an increase in cell size in *an3-4* plants. However, our data show that this response is suppressed by EODFR when PIF7 is present (Fig. 3*C*). This appears to be a PIF7-dependent compensatory mechanism to prevent leaf growth through cell expansion that would otherwise occur when AN3 is deactivated.

As EODFR led to a substantial reduction in *AN3* transcript levels, this indicated PIF7 may suppress *AN3* gene expression. This proposition was substantiated by genetic data, while ChIP-qPCR assays showed PIF7 can directly bind to a G-box–containing region of the *AN3* promoter (Fig. 4*C*). However, our results also showed that 35S::AN3 plants displayed a WT EODFR response, implying that PIF7 may also control AN3 through an alternative, posttranscriptional mechanism (Fig. 4*E*). The rationale being that if PIF7 acted solely through the transcriptional repression of *AN3*, then AN3 overexpression should block, or at least reduce, the impact of EODFR. Previous reports have shown that AN3 can self-regulate through a positive feedback loop by binding to the UTR-located GAGA motif and the CATGTT motif of its own promoter (26, 44, 47). Our ChIP-qPCR demonstrated that AN3 binding to these self-regulatory elements can be blocked by EODFR and that PIF7 is required for EODFR-induced AN3 promoter eviction (Fig. 4 *F–H*). These results therefore indicate that PIF7 may operate by removing AN3 from self-regulatory motifs. Concurring with this interpretation, our in vitro and in vivo co-IP assays illustrate that PIF7-Flash can directly bind AN3^{yellow}, suggesting that PIF7 may repress AN3 action through a sequestration-type mechanism (Fig. 4*I* and *SI Appendix*, Fig. S7*B*).

This functional property of PIF7 is reminiscent of mechanisms reported for HFR1, PAR1/2, HEC1/2, and DELLAs (48–51). HFR1, PAR1/2, and HEC1/2 are HLH proteins that, unlike PIF7, do not bind to DNA directly but have been shown to sequester DNA-binding PIFs through heterodimerization (49–52). Interestingly, we recorded slightly increased AN3 protein levels following EODFR (Fig. 4*I*). While we do not know if this results from the PIF7-AN3 interaction, sequestration has been shown to alter target protein stability. For example, DELLAs inhibit PIF binding to target genes by directly sequestering their DNA-recognition domains and by inducing PIF degradation through the ubiquitin–proteasome system (48). Similarly, HFR1 can sequester and promote the degradation of PIF1 and PIF5 in the dark in a heterodimerization-dependent manner (53). The PIF7 sequestration of AN3 potentially leads to the buildup of inactive heterodimers. Interestingly, a comparable regulatory mechanism has recently been described for HEC2 control of PIF4 in thermomorphogenesis (54). Here, HEC2 both stabilizes PIF4 and inhibits PIF4 function through heterodimerization.

Our genetic data provide evidence that several key cell proliferation genes (*GRF1*, *GRF2*, *GRF3*, *GRF4*, *GRF5*, *GRF6*, *CYCB1;1*, *OLI2*, *STZ*, *CDC45*, and *CDC6*) are antagonistically regulated by AN3 and PIF7. As the known PIF7- and AN3-binding G-box/PBE-boxes were common motifs found in the promoters of all these genes, this suggested PIF7 and AN3 signal convergence at common motifs (26, 41). ChIP-qPCR assays showed that this was indeed the case and that EODFR induced switching from AN3 to PIF7 enrichment. The loss of AN3 eviction in the *pif7-1* mutant confirmed that AN3 binding at G-box/PBE-boxes is dependent on the absence of active PIF7 (Fig. 5*C* and *SI Appendix*, Fig. S9*C*). The opposing action of AN3 and PIF7 on target gene expression means that the EODFR-induced substitution mechanism facilitates the on to off modulation of gene expression.

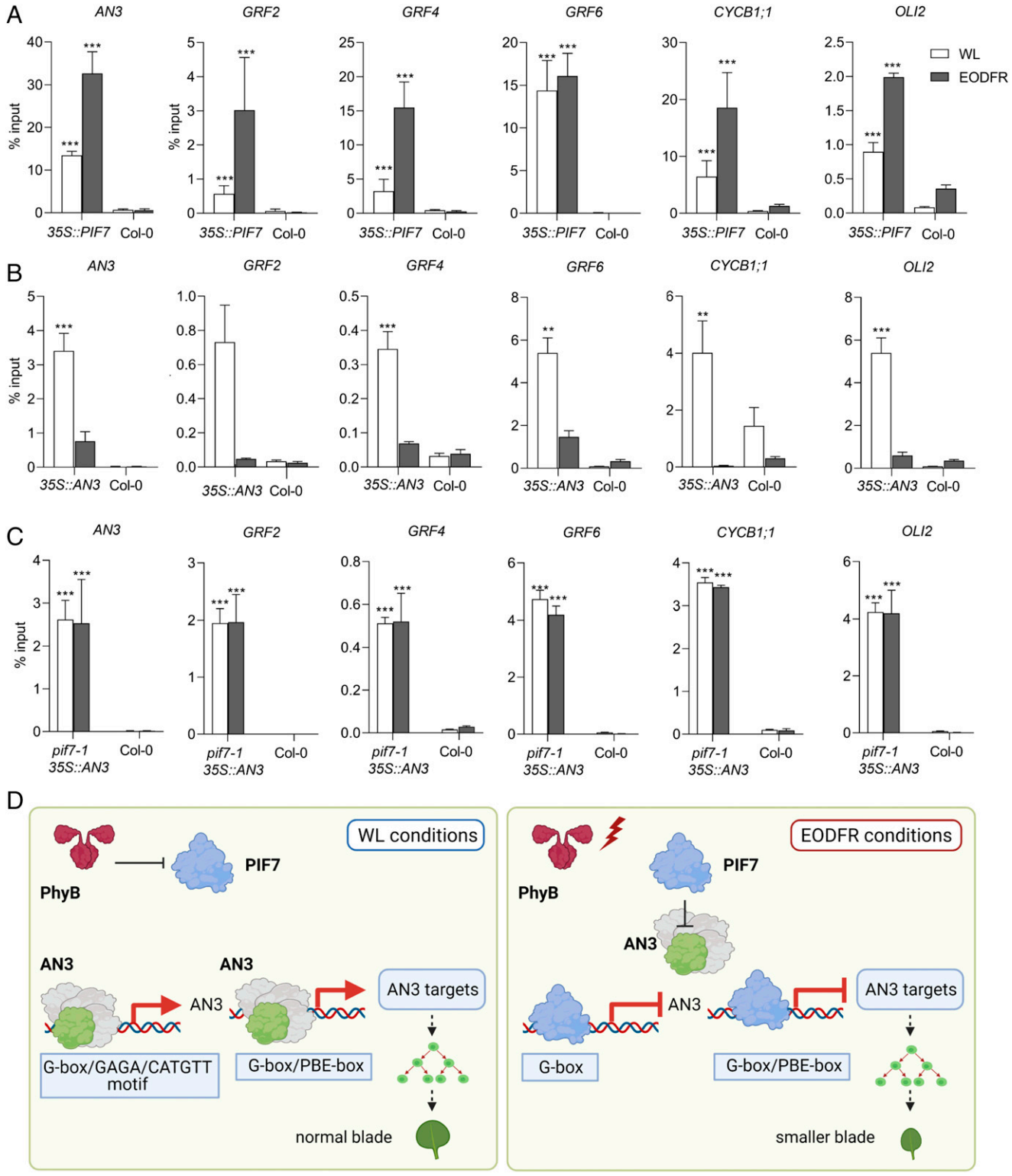

Fig. 5. AN3 association with target gene promoters is PIF7 dependent following EODFR. (*A–C*) ChIP assays showing EODFR controlled PIF7-FLASH or AN3^{yellow} enrichment at G-box or PBE regions of AN3 target genes (*AN3*, *GRF2*, *GRF4*, *GRF6*, *CYCB1;1*, and *OLI2*). PIF7-FLASH enrichment in the *35S::PIF7-FLASH (35S::PIF7)* line is compared to Col-0 (WT) (*A*). AN3^{yellow} enrichment in the *35S::AN3^{yellow} (35S::AN3)* line is compared to *pif7-1;35S::AN3^{yellow} (pif7-1;35S::AN3)* and Col-0 (WT) (*B* and *C*). Samples were taken at ZT14 from 13-d-old seedlings grown at 22 °C. Mean values are shown, error bars represent the SD of three biological replicates (*$P < 0.05$, **$P < 0.01$, and ***$P < 0.001$, Student's *t* test). (*D*) Schematic depicting PIF7 control of leaf cell proliferation through an AN3 substitution repression mechanism. In control conditions, phyB suppresses PIF7 activity, and the AN3 complex is able to bind to G-box/GAGA/CATGTT regions of its own promoter/UTR and G-box/PBE regions of other target promoters to promote their expression. EODFR deactivation of phyB leads to the de-repression of PIF7, which can then sequester AN3 and substitute for AN3 at G-box/PBE promoter motifs. This EODFR-elicited substitution mechanism leads to the suppression of gene expression and leaf cell proliferation.

Interestingly, analogous behavior has previously been reported for AN3, which can competitively interact with JANUS to inhibit its Pol II recruitment on the *PLT1* promoter and antagonistically regulate *PLT1* transcription in the root meristem (55). Furthermore, the opposing action has been observed for PIF1/3 and the bZIP transcription factors HY5 and HYH, which can physically interact and can bind to G-box–containing regions in a common set of target promoters (56, 57). Our findings also have similarities to the recently reported PIF3-TCP4 substitution–suppression module (58). In this instance, darkness-induced accumulation of PIF3 in seedling cotyledons triggers the substitution of TCP4 for PIF3 at shared *cis*-elements in *SAUR* gene promoters (58). As for the PIF7-AN3 module, conditional switching between PIF1/3 and HY5/HYH or PIF3 and TCP4 promoter occupancy provides a mechanism through which external signals can direct changes in gene expression.

Previously, PIF7 has been shown to participate in transcriptional activation of key SAS genes including *YUC8*, *YUC9*, *IAA19*, *IAA29*, *ATHB2*, and *PRE1* (16, 40, 43). PIF7 can directly interact with MORF-RELATED GENE 2 to promote histone acetylation and the expression of *YUC8*, *IAA19*, and *PRE1* (43). Recently, PIF7 and other PIFs were shown to control H2A.Z gene occupancy and H3K9 acetylation of the SAS genes *ATHB2*, *ATHB4*, *HAT2*, and *HAT3* (59). The activation of PIF7 by low R:FR triggers PIF7-DNA binding, H2A.Z removal, and target gene activation. In this study, we have shown PIF7 acts as a transcriptional repressor as it does in the regulation of the DRE-Binding1 C-repeat binding factor (60). Interestingly, PIF3 and PIF1 have both been reported to interact with HISTONE DEACETYLASE 15 (HDA15) to repress gene expression (61, 62). The mode of action through which PIF7 deactivates AN3 and suppresses target gene expression also has similarities to the well-studied mammalian *hairy and enhancer of split-1/Hairy/enhancer-of-split related with YRPW* (*tetrapeptide*)*motif protein* (*hes/hey*) system. Hes and Hey are bHLH notch-signaling proteins closely related to the *Drosophila hairy/enhancer of split* family of genes (63). Like PIFs, Hes and Hey proteins preferentially bind DNA at E-Box (CANNTG) variants, including the G-Box. Previous studies indicate that Hes and Hey mainly act as corepressors by interacting with and suppressing the activity of transcription factors and through the recruitment of deacetylases (63–66). It will be interesting to establish if the PIF7-mediated AN3 promoter eviction and transcriptional suppression represent an analogous process that is conserved across species.

In conclusion, this study shows that PIF7 inhibits leaf cell proliferation by inactivating the central leaf developmental regulator AN3. EODFR-activated PIF7 represses *AN3* expression by directly interacting with and sequestering AN3 from *cis*-elements in its own promoter. We show that PIF7 and AN3 signaling converges at G-box/PBE-box promoter elements in a major set of genes that control cell division. EODFR treatment induces the substitution of AN3 for PIF7 at target promoters and, vitally, a switch from promotion to repression of cell-cycle gene expression.

Materials and Methods

Plant Material and Growth Conditions. All *Arabidopsis thaliana* mutants and transgenic plants that were used in this study were from the Columbia (Col-0) ecotype. Some of the mutant and overexpressing lines used in this study were described elsewhere, including PIF7-Flash (35S::PIF7-Flash; 9xMyc-6xHis-3xFlag) (20) and 35S::AN3-GS^{yellow} (28). The triple mutant *grf1-3;grf3-1;grf5-2* and quintuple mutant *grf1-3;grf3-1;grf4-1;grf5-2* have been previously described elsewhere (67). The *phyB-9* (68), *pif7-1* (69), *pif1-2*, *pif3-3*, *pif4-2*, and *pif5-2* (*pifq*) (70) have been previously characterized. *an3-4* is an AN3-null mutant derived from an X-ray–irradiated population of the Col-0 accession (25).Other mutant combinations included *an3-4;phyB-9*, which were obtained by crossing *an3-4* with *phyB-9* plants, *an3-4;pif7-1* were obtained by crossing *an3-4* with *pif7-1* plants, and the triple *an3-4;phyB-9;pif7-1* mutant was obtained by crossing *an3-4;phyB-9* with *an3-4;pif7-1* plants. The *35S::PIF7-Flash; 35S::AN3-GS^{yellow}* plants were generated by crossing *35S::PIF7-Flash* with *35S::AN3-GS^{yellow}* plants, and double-homozygous transgenic plants were screened using 30 μg · ml^{-1} hygromycin and 50 μg · ml^{-1} kanamycin. *pif7-1;35S::AN3-GS^{yellow}* plants were made by crossing *35S::AN3-GS^{yellow}* with *pif7-1* plants. Presence of the *an3-4* and *pif7-1* mutations was identified by PCR, while the *phyB-9* mutation was confirmed by Sanger sequencing. The absence of the secondary *VENOSA4* mutation (71) was confirmed by sequencing. All primers used in this work are listed in *SI Appendix*, Table S1.

Seeds were sown on F2 + S Levington Advance Seed and Modular Compost plus sand soil mix (ICL Specialty Fertilizers) and stratified for 4 d in darkness at 4 °C. Seedlings were grown in a Percival SE-41L cabinet (CLF Plant Climatics) under control conditions: LD 12-h:12-h photoperiod at a 100 μmol · m^{-2} · s^{-1} fluence rate and constant temperature of 22 °C. Plants were either kept in control conditions or exposed to daily EODFR for 10 min after dusk (40 μmol · m^{-2} · s^{-1}) for periods of time (see figure legends). Sampling occured on day 34. For EODFR treatments, we used seven 24V OSLON 150 ILS-OW06-FRED-SD111 FR light-emitting diode (LED) strips (Intelligent Led Solutions) to deliver 40 μmol · m^{-2} · s^{-1} of FR light (730 nm) for 10 min each day. The spectrum of both light sources can be found in *SI Appendix*, Fig. S11. All reagents used in this work were purchased from Merck KGaA unless otherwise specified. Further growth condition details are provided in the respective figure legends.

Blade Area Measurement. Whole-leaf pictures for blade area measurements were taken from a fixed camera stand using a Nikon G20 camera with automatic focus settings (6). A ruler was included in each photograph for scaling purposes. Blade area was measured using NIH ImageJ software (https://rsb.info.nih.gov/nih-image/). The bar charts and box plots were generated using Prism 8 (GraphPad Software).

Generation of Transparent Leaf Blades for Microscopy Imaging. Leaf blades were excised from 34 D.A.S plants with a razor blade and cleared as described in ref. 6. The blades were then mounted onto microscope slides with the adaxial layer facing down.

Cell Size and Number Measurement. For epidermal and palisade cell parameter determination, cleared blades (34 d after sowing [D.A.S.]) were mounted and visualized using an Eclipse E600 (Nikon) Differential Inference Contrast (DIC) microscope using either a 10 or a 20× objective. Individual abaxial epidermal and adaxial subepidermal palisade cell sizes were measured using NIH ImageJ software (https://rsb.info.nih.gov/nih-image/). Average leaf cell sizes were obtained by deriving the mean values of nine adjacent cells from the base, the middle, and the tip sections of each leaf or these sections combined. The mean total number of cells was obtained by dividing the blade area by the total cell size of each blade and then averaging the mean total number of cells of each blade. The average cell density was obtained by dividing the total number of cells by the blade area and then averaging the mean cell density of each blade (6). An S8 stage mic 1 mm/0.01 mm graticule (no. 02A00404, Pyser-SGI Ltd.) was used for scaling. The bar charts and box plots were generated using Prism 8 (GraphPad Software).

RNA Extraction and RT-qPCR. For gene expression analysis, plants were grown for 13 d under an LD 12-h:12-h photoperiod, at 100 μmol · m^{-2} · s^{-1} fluence rate and 22 °C of constant temperature. On day 13, the plants were either shifted to daily EODFR (40 μmol · m^{-2} · s^{-1}) FR light for 10 min after dusk or kept in 100 μmol · m^{-2} · s^{-1} white light condition. Briefly, 13-d-old whole seedlings were harvested at zeitgeber 14 (ZT) in RNAlater solution (Thermo Fisher), and leaf 3 blades were dissected with a razor in a Petri dish filled with RNAlater solution (Sigma-Aldrich) under a Leica MZ 16 F dissecting microscope. Total RNA was extracted using the RNeasy Plant Mini Kit (Qiagen) with on-column DNase enzymatic digestion. All samples were processed on the same day. Complementary DNA (cDNA) synthesis was performed using the qScript cDNA SuperMix (Quanta Biosciences) as described by the manufacturer. The RT-qPCR was set up as a 10-μL reaction using Lightcycler 480 Synergy Brands Inc. (SYBR) Green Master Mix (Roche) in a 384-well plate, and performed with a Lightcycler 480 system (Roche). The results were analyzed using the Light Cycler 480 software. Gene-specific primers are listed in *SI Appendix*, Table S1. The bar charts were generated using Prism 8 (GraphPad Software).

ChIP-qPCR Assay. For ChIP-qPCR assays, plants were grown for 13 d under an LD 12h:12-h photoperiod at 100 μmol · m^{-2} · s^{-1} fluence rate and 22 °C of constant temperature. On day 13, plants were either shifted to EODFR of 40 μmol m^{-2} s^{-1} FR light or kept in the 100 μmol · m^{-2} · s^{-1} white light condition. In all genotypes and treatments, 13-d-old whole seedling shoots were harvested at ZT14, 2 h after the EODFR pulse. The sample collection time of ZT14 was selected to capture a potential switch in AN3/PIF7 binding following EODFR treatment. The ChIP analyses protocol was adapted from ref. 72.

Briefly, whole aboveground seedlings were fixed under vacuum for 15 min repeated twice at 25 PSI in 1× phosphate buffered saline (PBS) containing 1% formaldehyde. The reaction was quenched by adding 2 M glycine to a final concentration of 125 mM and incubated for 5 min. The samples were washed three times in sterile MilliQ H_2O and ground to a fine powder with liquid nitrogen. The nuclei were isolated in three steps with the series of extraction buffers EB1-3. The lysate was centrifugated at 4,000 rpm at 4 °C for 20 min in EB1 (0.4 M sucrose, 10 mM Tris HCl [pH8], 10 mM $MgCl_2$, 5 mM 2-mercaptoethanol [BME], 0.2 mM phenylmethylsulfonyl fluoride [PMSF], 2 phosphatase inhibitor mini tablets, and 1 mM ethylene-diamine-tetraacetic acid (EDTA)), at 12,000 rpm for 10 min in EB2 (0.25 M sucrose, 10 mM Tris HCl [pH8], 10 mM $MgCl_2$, 5 mM BME, 0.2 mM PMSF, 1 complete minitablet, and 1 mM EDTA), and then at 15,000 rpm for 1 h in EB3 (1.7 M sucrose, 10 mM Tris HCl [pH8], 2 mM $MgCl_2$, 5 mM BME, 0.2 mM PMSF, 0.15% [vol/vol] Triton X-100, 1 complete minitablet, and 1 mM EDTA). Chromatin was extracted with cold nuclei lysis buffer (50 mM Tris HCl [pH8], 10 mM EDTA, 0.4 mM PMSF, 1 complete minitablet, 1% wt/vol sodium dodecyl sulphate (SDS)) after centrifugation at 4,000 rpm for 5 min. The chromatin solution was sonicated for 7 × 10 s, 5 × 10 s, and 3 × 10 s at power setting 9. The chromatin solution was diluted to reduce the 1% SDS to 0.1% SDS with ChIP buffer (16.7 mM Tris HCl [pH8], 167 mM NaCl, 0.2 mM PMSF, 1.1% [vol/vol] Triton X-100, 2.5 complete minitablet, and 1.2 mM EDTA). The chromatin complexes were immunoprecipitated with an anti-GFP antibody (ab290) and an anti-myc mouse antibody (mAb 9E10, Calbiochem) with a concentration of 2 μg/sample and incubated in ChIP dilution buffer with 20 μL Dynabeads Protein A (Thermo Fisher) overnight at 4 °C. An equal amount of chromatin solution was not treated with antibody and thus served as the mock antibody control. The beads were washed for 5 min each time at 4 °C with 1 ml each of the following buffers: two times with low salt wash buffer (150 mM NaCl, 20 mM Tris HCl [pH8], 0.1% wt/vol SDS, 1% vol/vol Triton X-100, and 2 mM EDTA), two times with high salt wash buffer (500 mM NaCl, 20 mM Tris HCl [pH 8], 0.1% wt/vol SDS, 1% vol/vol Triton X-100, and 2 mM EDTA), two times with LiCl wash buffer (0.25 M LiCl, 1% wt/vol sodium deoxycholate, 10 mM Tris HCl [pH8], 1% vol/vol Nonidet P-40, and 1 mM EDTA), and two times with Tris-EDTA (TE) buffer (1 mM EDTA and 10 mM Tris HCl [pH8]). DNA was extracted from the beads with elution buffer containing 1% wt/vol SDS and 0.1 M $NaHCO_3$ at 65 °C for 15 min and reversely cross-linked with 192 mM NaCl at 65 °C overnight. The proteins were removed with an equal volume of phenol:chloroform:isoamyl-alcohol (25:24:1). An additional step was performed by incubating the chromatin solution for 1 h at 45 °C in a buffer solution containing 0.5 M EDTA, 1 M Tris HCl (pH6.5), and 10 mg/mL proteinase K to elute and remove any of the remaining proteins. DNA was precipitated with a 2.5 volume of 100% ethanol, 1 μl glycogen, 1/10 volume of 1.5 M potassium acetate (pH 5.2) and spun at 15,000 rpm for 30 min. The supernatant was removed, and the DNA pellet was dried with 70% ethanol. A small aliquot of the untreated sonicated chromatin was reverse cross-linked for use as the total input DNA control. The ChIP assays were quantified by qPCR after normalizing with the input DNA. Gene-specific primers covering the G-box and PBE-box are listed in *SI Appendix*, Table S1. The bar charts were generated using Prism 8 (GraphPad Software).

In Vivo Co-IP Assays. For co-IP assays, plants were grown for 13 d under an LD 12h:12-h photoperiod at 100 $\mu mol \cdot m^{-2} \cdot s^{-1}$ fluence rate and 22 °C of constant temperature. On day 13, plants were either shifted to EODFR of 40 $\mu mol \cdot m^{-2} \cdot s^{-1}$ FR light or kept in 100 $\mu mol \cdot m^{-2} \cdot s^{-1}$ white light condition. Whole seedling shoots of *35S::PIF7-Flash;35S::AN3-GS^{yellow}* double overexpressor and *35S::AN3-GS^{yellow}* single overexpressor were harvested in liquid nitrogen at ZT14. The co-IP was performed following the method of Zhu et al. (73). Briefly, samples were ground to a fine powder in liquid nitrogen and homogenized in two volumes (mg/μL) of co-IP buffer containing 100 mM phosphate buffer, pH 7.8, 150 mM NaCl, 0.1% Nonidet P-40, 1× protease inhibitor mixture, 1 mM PMSF, 10 mM iodoacetamide, 40 μM bortezomib, 25 mM β-glycerophosphate, 10 mM sodium fluoride, and 2 mM sodium orthovanadate. After centrifugation at 15,000 rpm for 15 min at 4 °C in the dark, total protein levels were quantified with the Bradford Protein Assay (Bio-Rad), and the lysate was incubated with anti-Myc antibody precoupled Dynabeads Protein A (Thermo Fisher) for 4 h at 4 °C. The samples were precipitated with anti-Myc antibody and ran on a 4 to 12% NuPAGE Bis-Tris gel (Thermo Fisher) and blotted using the MiniBlot Module (Life Technologies) at 20 V for 1 h. Western blot detection for 35S::PIF7-Flash was performed using anti-Myc 9B11 (Cell Signaling) 1:1,000 and anti-Mouse IgG (whole molecule) peroxidase antibody (A4416 Sigma) 1:10,000. Western blot detection for 35S::AN3-GS^{yellow} was performed using an anti-GFP antibody (ab290) 0.1:1,000 and Goat Anti-Rabbit IgG H&L (HRP) (ab6721) 1:10,000.

In Vitro Co-IP Assays. For in vitro IP assays, the method of Paik et al. (74) was adopted with slight modifications. Briefly, 35S::PIF7-Flash and 35S::AN3-GS^{yellow} seeds were grown as described in *In Vivo Co-IP Assays*. Total protein was solubilized in pulled-down buffer (125 mM Tris HCl, pH7.7, 0.25 mM EDTA, 150 mM NaCl, 5% Glycerol, 0.1% Triton, 1× protease inhibitor mixture [Sigma-Aldrich Co., Catalogue no. P9599], 1× Halt phosphatase inhibitor mixture [Thermo Fisher, Cat no. 78420]. The extracts were cleared by centrifugation at 8,500 g for 12 min at 4 °C in the dark. The supernatant was incubated with 20 μL anti-GFP [GFP-Trap Magnetic Agarose, gtma-20, Chromotek] and Anti-FLAG M2 [Sigma, Cat no. M8823-1ML] magnetic beads for 2 h in an orbital shaker at 4 °C in the dark). Immunoprecipitated proteins were washed five times with pulled-down buffer (without inhibitors). Individually pulled-down proteins were mixed and then subjected to co-IP with Anti-FLAG M2 (Sigma, Cat no; M8823-1ML) magnetic beads. Beads were then boiled with 2× SDS sample buffer (80 mM Tris HCL, pH 6.8, 2% SDS, 10% glycerol, 0.0006% bromophenol blue, and 0.1 M dithiothreitol [DTT]) at 85 °C for 10 min and separated on an sodium dodecyl sulphate–polyacrylamide gel electrophoresis (SDS-PAGE) gel. Primary antibodies, an anti-GFP (abcam, Cat no. 290), anti-Myc (anti-Myc 9B11 [Cell Signaling Technology (CST)]), and secondary antibodies (HRP [ab6721], anti-mouse-HRP [no. 7076, CST] were used to detect coimmunoprecipitated proteins).

Promoter Analysis. A 2-kb upstream promoter region of each target gene was obtained using PlantPAN 3.0 (http://plantpan.itps.ncku.edu.tw/). Regions were manually searched for G-box (CACGTG) and PBE-box (CA[TG/CA]TG) target-binding sites.

Statistical Information. The statistical difference of two populations was tested by two-tailed, unpaired Student's *t* test. To compare three or more populations, a one-way ANOVA followed by Tukey's test (comparison among all groups) was performed. When Tukey's test was employed, letters were used to indicate which treatment groups were significantly different. All analyses were performed using GraphPad Prism 8.0.2 (GraphPad Software) or Minitab 19 (Minitab Ltd.) unless otherwise indicated.

Data Availability. All study data are included in the article, the *SI Appendix* and Array Express (https://www.ebi.ac.uk/arrayexpress/experiments/E-MTAB-9445/?query=Romanowski).

ACKNOWLEDGMENTS. We thank Prof. Dirk Inzé for providing us with the *35S::AN3-GS^{yellow}* line, Prof. Gorou Horiguchi for *an3-4* seeds, Prof. Jeong Hoe Kim for *grf1-3;grf3-1;grf5-2*, *grf1-3;grf3-1; grf4-1;grf5-2* seeds, and Prof. Joanne Chory and Dr. Elena Monte for *35S::PIF7-Flash* line. We would like to thank Prof. Enamul Huq, Dr. Beatriz Orosa, Dr. Imtiyaz Yaseen, Dr. Gabriela Toledo-Ortiz and Dr. Michael Skelly for advice on molecular assays, and also M. E. Goya for her help with BioRender. E.H. was funded by the Punjab Educational Endowment Fund PEEF/CMMS/2016/203. This work was supported by United Kingdom Research and Innovation, Biotechnology, and Biological Sciences Research Council Grants BB/M025551/1 and BB/N005147/1 awarded to K.J.H.

1. G. Sessa, M. Carabelli, M. Possenti, G. Morelli, I. Ruberti, Multiple pathways in the control of the shade avoidance response. *Plants* **7**, 102 (2018).
2. D. Yang, D. D. Seaton, J. Krahmer, K. J. Halliday, Photoreceptor effects on plant biomass, resource allocation, and metabolic state. *Proc. Natl. Acad. Sci. U.S.A.* **113**, 7667–7672 (2016).
3. J. Krahmer *et al.*, Phytochromes control metabolic flux, and their action at the seedling stage determines adult plant biomass. *J. Exp. Bot.* **72**, 3263–3278 (2021).
4. D. Patel *et al.*, Temperature-dependent shade avoidance involves the receptor-like kinase ERECTA. *Plant J.* **73**, 980–992 (2013).
5. M. Carabelli *et al.*, Arabidopsis HD-Zip II proteins regulate the exit from proliferation during leaf development in canopy shade. *J. Exp. Bot.* **69**, 5419–5431 (2018).
6. A. Romanowski, J. J. Furniss, E. Hussain, K. J. Halliday, Phytochrome regulates cellular response plasticity and the basic molecular machinery of leaf development. *Plant Physiol.* **186**, 1220–1239 (2021).
7. K. A. Franklin, P. H. Quail, Phytochrome functions in Arabidopsis development. *J. Exp. Bot.* **61**, 11–24 (2010).
8. C. Klose, F. Nagy, E. Schäfer, Thermal reversion of plant phytochromes. *Mol. Plant* **13**, 386–397 (2020).
9. K. A. Franklin, G. C. Whitelam, Light signals, phytochromes and cross-talk with other environmental cues. *J. Exp. Bot.* **55**, 271–276 (2004).
10. M. J. Yanovsky, J. J. Casal, G. C. Whitelam, Phytochrome A, phytochrome B and HY4 are involved in hypocotyl growth responses to natural radiation in Arabidopsis:

Weak de-etiolation of the phyA mutant under dense canopies. *Plant Cell Environ.* **18**, 788–794 (1995).
11. E. Park *et al.*, Phytochrome B inhibits binding of phytochrome-interacting factors to their target promoters. *Plant J.* **72**, 537–546 (2012).
12. E. Park, Y. Kim, G. Choi, Phytochrome B requires PIF degradation and sequestration to induce light responses across a wide range of light conditions. *Plant Cell* **30**, 1277–1292 (2018).
13. V. N. Pham, P. K. Kathare, E. Huq, Phytochromes and phytochrome interacting factors. *Plant Physiol.* **176**, 1025–1038 (2018).
14. X. Huang *et al.*, Shade-induced nuclear localization of PIF7 is regulated by phosphorylation and 14-3-3 proteins in *Arabidopsis. eLife* **7**, e31636 (2018).
15. M. G. Salter, K. A. Franklin, G. C. Whitelam, Gating of the rapid shade-avoidance response by the circadian clock in plants. *Nature* **426**, 680–683 (2003).
16. T. Mizuno, H. Oka, F. Yoshimura, K. Ishida, T. Yamashino, Insight into the mechanism of end-of-day far-red light (EODFR)-induced shade avoidance responses in Arabidopsis thaliana. *Biosci. Biotechnol. Biochem.* **79**, 1987–1994 (2015).
17. K. A. Franklin, Shade avoidance. *New Phytol.* **179**, 930–944 (2008).
18. B. Strasser, M. Sánchez-Lamas, M. J. Yanovsky, J. J. Casal, P. D. Cerdán, Arabidopsis thaliana life without phytochromes. *Proc. Natl. Acad. Sci. U.S.A.* **107**, 4776–4781 (2010).
19. P. Leivar *et al.*, Phytochrome-imposed inhibition of PIF7 activity shapes photoperiodic growth in Arabidopsis together with PIF1, 3, 4 and 5. *Physiol. Plant.* **169**, 452–466 (2020).
20. L. Li *et al.*, Linking photoreceptor excitation to changes in plant architecture. *Genes Dev.* **26**, 785–790 (2012).
21. Y. Jiang *et al.*, The ELF3-PIF7 interaction mediates the circadian gating of the shade response in Arabidopsis. *iScience* **22**, 288–298 (2019).
22. M. Carabelli *et al.*, Canopy shade causes a rapid and transient arrest in leaf development through auxin-induced cytokinin oxidase activity. *Genes Dev.* **21**, 1863–1868 (2007).
23. H. Tsukaya, T. Kozuka, G. T. Kim, Genetic control of petiole length in Arabidopsis thaliana. *Plant Cell Physiol.* **43**, 1221–1228 (2002).
24. J. H. Kim, H. Kende, A transcriptional coactivator, AtGIF1, is involved in regulating leaf growth and morphology in Arabidopsis. *Proc. Natl. Acad. Sci. U.S.A.* **101**, 13374–13379 (2004).
25. G. Horiguchi, G. T. Kim, H. Tsukaya, The transcription factor AtGRF5 and the transcription coactivator AN3 regulate cell proliferation in leaf primordia of Arabidopsis thaliana. *Plant J.* **43**, 68–78 (2005).
26. L. Vercruyssen *et al.*, ANGUSTIFOLIA3 binds to SWI/SNF chromatin remodeling complexes to regulate transcription during Arabidopsis leaf development. *Plant Cell* **26**, 210–229 (2014).
27. H. Nelissen *et al.*, Dynamic changes in ANGUSTIFOLIA3 complex composition reveal a growth regulatory mechanism in the maize leaf. *Plant Cell* **27**, 1605–1619 (2015).
28. N. Besbrugge *et al.*, GS^{yellow}, a multifaceted tag for functional protein analysis in monocot and dicot plants. *Plant Physiol.* **177**, 447–464 (2018).
29. S. Shimano *et al.*, Conserved functional control, but distinct regulation, of cell proliferation in rice and *Arabidopsis* leaves revealed by comparative analysis of *GRF-INTERACTING FACTOR 1* orthologs. *Development* **145**, dev159624 (2018).
30. T. Kozuka *et al.*, The different growth responses of the Arabidopsis thaliana leaf blade and the petiole during shade avoidance are regulated by photoreceptors and sugar. *Plant Cell Physiol.* **46**, 213–223 (2005).
31. M. Andriankaja *et al.*, Exit from proliferation during leaf development in Arabidopsis thaliana: A not-so-gradual process. *Dev. Cell* **22**, 64–78 (2012).
32. M. Beltramino *et al.*, Robust increase of leaf size by Arabidopsis thaliana GRF3-like transcription factors under different growth conditions. *Sci. Rep.* **8**, 13447 (2018).
33. N. Gonzalez, H. Vanhaeren, D. Inzé, Leaf size control: Complex coordination of cell division and expansion. *Trends Plant Sci.* **17**, 332–340 (2012).
34. B. H. Lee *et al.*, The Arabidopsis GRF-INTERACTING FACTOR gene family performs an overlapping function in determining organ size as well as multiple developmental properties. *Plant Physiol.* **151**, 655–668 (2009).
35. J. Van Leene *et al.*, Targeted interactomics reveals a complex core cell cycle machinery in Arabidopsis thaliana. *Mol. Syst. Biol.* **6**, 397 (2010).
36. K. Kawade, G. Horiguchi, T. Usami, M. Y. Hirai, H. Tsukaya, ANGUSTIFOLIA3 signaling coordinates proliferation between clonally distinct cells in leaves. *Curr. Biol.* **23**, 788–792 (2013).
37. D. Liebsch, J. F. Palatnik, MicroRNA miR396, GRF transcription factors and GIF coregulators: A conserved plant growth regulatory module with potential for breeding and biotechnology. *Curr. Opin. Plant Biol.* **53**, 31–42 (2020).
38. M. Nozaki, K. Kawade, G. Horiguchi, H. Tsukaya, an3-mediated compensation is dependent on a cell-autonomous mechanism in leaf epidermal tissue. *Plant Cell Physiol.* **61**, 1181–1190 (2020).
39. Y. Xie *et al.*, Phytochrome-interacting factors directly suppress MIR156 expression to enhance shade-avoidance syndrome in Arabidopsis. *Nat. Commun.* **8**, 348 (2017).
40. M. de Wit, K. Ljung, C. Fankhauser, Contrasting growth responses in lamina and petiole during neighbor detection depend on differential auxin responsiveness rather than different auxin levels. *New Phytol.* **208**, 198–209 (2015).
41. V. C. Galvão *et al.*, PIF transcription factors link a neighbor threat cue to accelerated reproduction in Arabidopsis. *Nat. Commun.* **10**, 4005 (2019).
42. Z. Liu, N. Li, Y. Zhang, Y. Li, Transcriptional repression of GIF1 by the KIX-PPD-MYC repressor complex controls seed size in Arabidopsis. *Nat. Commun.* **11**, 1846 (2020).
43. M. Peng *et al.*, Linking phytochrome-interacting factor to histone modification in plant shade avoidance. *Plant Physiol.* **176**, 1341–1351 (2018).
44. L. S. Meng *et al.*, Arabidopsis ANGUSTIFOLIA3 (AN3) is associated with the promoter of CONSTITUTIVE PHOTOMORPHOGENIC1 (COP1) to regulate light-mediated stomatal development. *Plant Cell Environ.* **41**, 1645–1656 (2018).
45. D. C. Bergmann, F. D. Sack, Stomatal development. *Annu. Rev. Plant Biol.* **58**, 163–181 (2007).
46. J. Vercruysse, A. Baekelandt, N. Gonzalez, D. Inzé, Molecular networks regulating cell division during Arabidopsis leaf growth. *J. Exp. Bot.* **71**, 2365–2378 (2020).
47. J. H. Kim, Biological roles and an evolutionary sketch of the GRF-GIF transcriptional complex in plants. *BMB Rep.* **52**, 227–238 (2019).
48. K. Li *et al.*, DELLA-mediated PIF degradation contributes to coordination of light and gibberellin signalling in Arabidopsis. *Nat. Commun.* **7**, 11868 (2016).
49. P. Hornitschek, S. Lorrain, V. Zoete, O. Michielin, C. Fankhauser, Inhibition of the shade avoidance response by formation of non-DNA binding bHLH heterodimers. *EMBO J.* **28**, 3893–3902 (2009).
50. Y. Hao, E. Oh, G. Choi, Z. Liang, Z. Y. Wang, Interactions between HLH and bHLH factors modulate light-regulated plant development. *Mol. Plant* **5**, 688–697 (2012).
51. L. Zhu *et al.*, A negative feedback loop between PHYTOCHROME INTERACTING FACTORs and HECATE proteins fine-tunes photomorphogenesis in Arabidopsis. *Plant Cell* **28**, 855–874 (2016).
52. H. Shi *et al.*, HFR1 sequesters PIF1 to govern the transcriptional network underlying light-initiated seed germination in Arabidopsis. *Plant Cell* **25**, 3770–3784 (2013).
53. X. Xu *et al.*, Reciprocal proteasome-mediated degradation of PIFs and HFR1 underlies photomorphogenic development in *Arabidopsis. Development* **144**, 1831–1840 (2017).
54. S. Lee, L. Zhu, E. Huq, An autoregulatory negative feedback loop controls thermomorphogenesis in Arabidopsis. *PLoS Genet.* **17**, e1009595 (2021).
55. F. Xiong *et al.*, Transcriptional regulation of *PLETHORA1* in the root meristem through an importin and its two antagonistic cargos. *Plant Cell* **32**, 3812–3824 (2020).
56. D. Chen *et al.*, Antagonistic basic helix-loop-helix/bZIP transcription factors form transcriptional modules that integrate light and reactive oxygen species signaling in Arabidopsis. *Plant Cell* **25**, 1657–1673 (2013).
57. G. Toledo-Ortiz *et al.*, The HY5-PIF regulatory module coordinates light and temperature control of photosynthetic gene transcription. *PLoS Genet.* **10**, e1004416 (2014).
58. J. Dong *et al.*, The transcription factors tcp4 and pif3 antagonistically regulate organ-specific light induction of saur genes to modulate cotyledon opening during de-etiolation in arabidopsis. *Plant Cell* **31**, 1155–1170 (2019).
59. B. C. Willige *et al.*, PHYTOCHROME-INTERACTING FACTORs trigger environmentally responsive chromatin dynamics in plants. *Nat. Genet.* **53**, 955–961 (2021).
60. S. Kidokoro *et al.*, The phytochrome-interacting factor PIF7 negatively regulates DREB1 expression under circadian control in Arabidopsis. *Plant Physiol.* **151**, 2046–2057 (2009).
61. X. Liu *et al.*, PHYTOCHROME INTERACTING FACTOR3 associates with the histone deacetylase HDA15 in repression of chlorophyll biosynthesis and photosynthesis in etiolated Arabidopsis seedlings. *Plant Cell* **25**, 1258–1273 (2013).
62. D. Gu *et al.*, Identification of HDA15-PIF1 as a key repression module directing the transcriptional network of seed germination in the dark. *Nucleic Acids Res.* **45**, 7137–7150 (2017).
63. D. Weber, C. Wiese, M. Gessler, Hey bHLH transcription factors. *Curr. Top. Dev. Biol.* **110**, 285–315 (2014).
64. T. Iso, G. Chung, Y. Hamamori, L. Kedes, HERP1 is a cell type-specific primary target of Notch. *J. Biol. Chem.* **277**, 6598–6607 (2002).
65. T. Takata, F. Ishikawa, Human Sir2-related protein SIRT1 associates with the bHLH repressors HES1 and HEY2 and is involved in HES1- and HEY2-mediated transcriptional repression. *Biochem. Biophys. Res. Commun.* **301**, 250–257 (2003).
66. F. Gould, S. M. Harrison, E. W. Hewitt, A. Whitehouse, Kaposi's sarcoma-associated herpesvirus RTA promotes degradation of the Hey1 repressor protein through the ubiquitin proteasome pathway. *J. Virol.* **83**, 6727–6738 (2009).
67. S.-J. Lee *et al.*, GROWTH-REGULATING FACTOR and GRF-INTERACTING FACTOR specify meristematic cells of gynoecia and anthers. *Plant Physiol.* **176**, 717–729 (2018).
68. J. W. Reed, P. Nagpal, D. S. Poole, M. Furuya, J. Chory, Mutations in the gene for the red/far-red light receptor phytochrome B alter cell elongation and physiological responses throughout Arabidopsis development. *Plant Cell* **5**, 147–157 (1993).
69. P. Leivar *et al.*, Multiple phytochrome-interacting bHLH transcription factors repress premature seedling photomorphogenesis in darkness. *Curr. Biol.* **18**, 1815–1823 (2008).
70. P. Leivar *et al.*, The Arabidopsis phytochrome-interacting factor PIF7, together with PIF3 and PIF4, regulates responses to prolonged red light by modulating phyB levels. *Plant Cell* **20**, 337–352 (2008).
71. Y. Yoshida *et al.*, The Arabidopsis *phyB-9* mutant has a second-site mutation in the *VENOSA4* gene that alters chloroplast size, photosynthetic traits, and leaf growth. *Plant Physiol.* **178**, 3–6 (2018).
72. A. V. Gendrel, Z. Lippman, C. Yordan, V. Colot, R. A. Martienssen, Dependence of heterochromatic histone H3 methylation patterns on the Arabidopsis gene DDM1. *Science* **297**, 1871–1873 (2002).
73. L. Zhu, E. Huq, Characterization of light-regulated protein-protein interactions by in vivo coimmunoprecipitation (Co-IP) assays in plants. *Methods Mol. Biol.* **2026**, 29–39 (2019).
74. I. Paik *et al.*, A phyB-PIF1-SPA1 kinase regulatory complex promotes photomorphogenesis in Arabidopsis. *Nat. Commun.* **10**, 4216 (2019).